

An empirical line-by-line model for the infrared solar transmittance spectrum from 700 to 5000 cm⁻¹

F. Hase^{a,*}, P. Demoulin^b, A.J. Sauval^c, G.C. Toon^d, P.F. Bernath^e, A. Goldman^f,
J.W. Hannigan^g, C.P. Rinsland^h

^a*Institut für Meteorologie und Klimaforschung, Forschungszentrum Karlsruhe, Postfach 3640, D-76021 Karlsruhe, Germany*

^b*Institut d'Astrophysique et de Géophysique, allée du VI août, 17, bâtiment B5a, B-4000, Liège, Belgium*

^c*Observatoire Royal de Belgique, avenue circulaire, 3, B-1180, Bruxelles, Belgium*

^d*Jet Propulsion Laboratory, 4800 Oak Grove Drive, Pasadena, CA 91109, USA*

^e*Department of Chemistry, University of Waterloo, Waterloo, Ont., Canada N2L3G1*

^f*Department of Physics, University of Denver, Denver, CO 80208, USA*

^g*Atmospheric Chemistry Division, National Center for Atmospheric Research, P.O. Box 3000, Boulder, CO 80303, USA*

^h*NASA Langley Research Center, Hampton, VA 23681-2199, USA*

Received 14 September 2005; received in revised form 24 January 2006; accepted 6 February 2006

Abstract

An empirical line-by-line model for the infrared solar transmittance spectrum is presented. The model can be incorporated into radiative transfer codes to allow fast calculation of all relevant emission and absorption features in the solar spectrum in the mid-infrared region from 700 to 5000 cm⁻¹. The transmittance is modelled as a function of the diameter of the field-of-view centered on the solar disk: the line broadening due to solar rotation as well as center-to-limb variations in strength and width are taken into account for stronger lines. Applications of the model presented here are in the fields of terrestrial remote sensing in the mid-infrared spectral region when the sun is used as radiation source or scattered solar radiation contributes to the measured signal and in the fields of atmospheric radiative transfer algorithms which compute the propagation of infrared solar radiation in the terrestrial atmosphere.

© 2006 Elsevier Ltd. All rights reserved.

Keywords: Infrared spectroscopy; Atmospheric trace gases; Solar spectrum; Radiative transfer; Retrieval algorithms

1. Introduction

Infrared remote sensing provides a powerful method to examine the chemical composition of the terrestrial atmosphere [1]. The self-emission of the atmosphere provides sufficient signal for detailed analysis if a moderate spectral resolution is applied in the thermal infrared, whereas observations with highest spectral resolution and at higher wave numbers in the mid-infrared require higher radiances. The sun provides a hot background source and is therefore used by ground-based and balloon- or satellite-borne occultation

*Corresponding author. Tel.: +49 7247 82 2434; fax: +49 7247 82 4742.

E-mail address: frank.hase@imk.fzk.de (F. Hase).

measurements of atmospheric composition. As an example of ground-based measurements of atmospheric composition the global network of high-resolution ground-based Fourier transform infrared (FTIR) spectrometers organized within the framework of the Network for the Detection of Stratospheric Change (NDSC) [2–4] provides long-term spectroscopic observations of many trace gases. The deduced time series are available via the NDSC database and have been used successfully for trend analysis [5,6] and for the validation of satellite experiments [7]. Examples for high-resolution balloon-borne FTIR occultation sounders are the University of Denver solar spectrometer [8], the Mk IV instrument [9] and LPMA [10]. Space-borne occultation instruments include the FTIR spectrometer ATMOS which participated in several Shuttle campaigns [11] and the ACE FTS instrument operating onboard the SCISAT satellite since August 2003 [12].

The solar spectrum in the mid-infrared spectral region is far from a smooth blackbody spectrum but is strewn with absorption features generated by the temperature stratification across the solar photosphere. For the case of space-borne instruments, the solar background can be largely removed before the analysis of terrestrial features by ratioing against a pure solar spectrum taken at high solar elevations. A similar strategy can also be applied to spectra derived from balloon-borne instrumentation, but for case of ground-based measurements compatible spectra with negligible air mass are not available. For instance, ratioing ground-based absorption spectra against solar spectra measured by ATMOS to correct for the solar background is inadequate for several reasons:

- The spectral resolution of the ground-based instruments is generally higher, whereas narrow solar features are not fully resolved by ATMOS.
- The signal-to-noise ratio of the ground-based spectra is very good (as high as ~ 1000), so use of the ATMOS solar spectrum would introduce additional noise and spectral artifacts.
- Due to the variable speed between sun and observer and due to differences between the instruments concerning the spectral calibration, the ratioing cannot be performed before the analysis, but has to be included in the analysis procedure.

For ground-based measurements, it is therefore preferable to include a model of the solar absorption features in the forward model radiative transfer code. Other possible applications of the model presented here are calculations targeting the flux of infrared radiation in the atmosphere for e.g. non-LTE calculations [13] or scattering of solar radiation into the line of sight of an infrared sounder [14]. These kinds of applications require full disk solar spectra. Since the variability of the solar spectrum near the very limb is considerably larger, the quality of modelled spectra in this case will be somewhat reduced in comparison to applications which cover only the central part of the solar disk. The empirical model described here provides a solar transmittance spectrum; that assumes spectral lines on a smooth, slowly varying continuum and does not reproduce slow spectral variations of the continuum itself. This approach is chosen for two reasons: for many applications, such as in the NDSC work described above, only selected spectral windows are used and the absolute continuum value does not affect the analysis. Moreover, high-resolution measurements of the solar spectrum in the mid-infrared currently do not employ sufficient calibration to absolute radiances.

2. Model setup and input

The construction of an optimal solar transmittance model should start by collecting available measurements of the solar spectrum and should combine this material with theoretical expectations of the solar output derived from radiative transfer calculations through the solar atmosphere. Since the astrophysical calculations rely on databases of relevant transitions, a line-by-line model is the natural choice for the final empirical model also.

2.1. Observations

Table 1 lists the measurements that compose the empirical data used in the model formulation. The ATMOS solar spectra [15] are essentially free from terrestrial spectral features. Still, sparse spectral artifacts are even found in ATMOS spectra and are due to absorption by residual CO_2 and H_2O trapped inside the

Table 1
Solar measurements used for the setup of the empirical model

Measurement	Date	Spectral coverage (cm^{-1})	Spectral resolution (max. optical path difference in cm)	Field of view as fraction of solar disk diameter	Airmass (1.0 for vertical observation at sea level)
ATMOS Spacelab-3 mission spectra http://remus.jpl.nasa.gov/atmos/sl3.sun.html	1985, day 87	600–4800 (several filter bands)	49	0.11–0.28 (filter dependent)	0
ATMOS ATLAS-3 mission spectra http://remus.jpl.nasa.gov/atmos/ftp.at3.sun.html	1992, day 87	600–4800 (several filter bands)	49	0.11–0.22 (filter dependent)	0
Mk IV solar spectrum filter 1 (longwave)	1992, day 258	1700–5890	64	0.46	0.01
Mk IV solar spectrum filter 2 (shortwave)	1992, day 258	600–2490	64	0.39	0.01
ISSJ solar spectra filter 1	2001, Jan. 15	700–1360	82	0.025	1.7
ISSJ solar spectra filter 2	2001, Jan. 20	1800–2250	101	0.015	1.7
ISSJ solar spectra filter 3	2001, Jan. 14	1950–3230	101	0.015	1.7
ISSJ solar spectra filter 4	2001, Jan. 16	3900–5170	62	0.015	1.7
Izaña solar spectra filter S1	2005, Jan. 26	3950–4370	180	0.22	0.9
Izaña solar spectra filter S3	2005, Jan. 25	2460–3120	180	0.22	0.9
Izaña solar spectra filter S4	2005, Jan. 25	2020–2630	180	0.27	0.9
Izaña solar spectra filter S5	2005, Jan. 25	1850–2140	180	0.27	0.9

instrument itself [16]. Fortunately, these artifacts can easily be distinguished from the solar features due to the large spacecraft-induced Doppler shifts. Due to nonlinear response of the photo-conductive HgCdTe detector, the zero baselines of the ATMOS spectra are somewhat uncertain [17]. The balloon-borne Mk IV interferometer [18] produces spectra of higher SNR and smaller baseline offset due to use of a photo-voltaic InSb detector over most of the spectral region considered in this work. The spectral resolution is superior to ATMOS, but spectra are taken at float heights about 39 km and solar zenith angles of about 33° . Therefore, the pure solar spectrum is still significantly superimposed upon terrestrial spectral features in many regions. Ground-based measurements were taken at the high-altitude International Scientific Station of the Jungfrauoch (ISSJ, Switzerland) with an FTIR spectrometer developed at University of Liège [19] and at the Izaña site on Tenerife with a commercial 125HR Bruker spectrometer [20]. These measurements offer the highest resolution, but are dominated by terrestrial absorption features over wide regions. In the case of the measurements taken at ISSJ, the solar radiation is guided to the spectrometer via a large astronomical telescope so the field of view on the solar disk is quite small, about 2 arcmin (1% of the apparent solar diameter). The small field and high tracking quality made it possible to take solar spectra not only at the center of the solar disk, but also at 0.6 times the projected disk radius to the East and West. In the case of the measurements taken at Izaña, the field of view is larger, about 0.1° or 20% of the apparent solar diameter and smaller de-centers of 0.2 times the projected disk radius have been applied.

2.2. Astrophysical linelist and solar radiative transfer calculations

Two ingredients serve as a starting point for the empirical line-by-line model: an astrophysical solar linelist and results from solar radiative transfer calculations to generate synthetic solar spectra as well as tables listing line area, half-width and residual intensity for each line in the calculated spectra. Both of these essential inputs to the empirical model have been provided by Sauval [21] and are described in the following.

2.2.1. Astrophysical solar linelist

The creation of an empirical model of the solar spectrum as presented here is clearly not the primary intended application of the astrophysical solar linelist, but is an interdisciplinary spin-off. The intended purpose of the astrophysical linelist will be in the calculation of solar and stellar infrared spectra, as the calculation of synthetic solar spectra based on photospheric models does require a set of accurate data for any relevant line. At present, no database is available which includes all the needed line parameters and especially there is a lack of accurate gf -values for atomic transitions. The near-infrared part of the astrophysical linelist is still under construction. The final list will encompass the spectral range from 250 to 10 000 cm^{-1} [21]. A preliminary version (2000) of this solar database has already been used in the calculation of spectra of cool stars in order to interpret a dozen spectra recorded by ISO (Infrared Space Observatory). First results [22,23] do show good agreement between observed and synthetic spectra which proves suitability of the new database to the calculation of stellar spectra also.

The astrophysical linelist is essentially based on the ATMOS linelist compiled by Geller [24] that is comprised of 15 400 solar features measured in the ATMOS spectra from 625 to 4800 cm^{-1} but fails to give two important quantities for any line: the lower state energy (the excitation potential) and the line intensity (gf -value). Moreover, about 2500 solar lines (very probably of atomic origin) remain unidentified. About 5300 solar lines of atomic origin are present in the infrared solar spectrum from 2 to 16 μm , with only about half of them clearly identified by Geller. Among the 2750 identified lines, there are 1200 lines attributed to neutral Fe, 640 to Si, 250 to Mg, 160 to C, etc. Most of these lines are of rather high excitation and as yet not observed in the laboratory. Moreover, gf -values are available in the literature for only a very small number of them. Improved and corrected identification lists of atomic lines have also been prepared by Geller in 1995 and in 1998. A computer file was generated in 1998 by G. Toon (JPL) based on Geller's updated 1998 linelist. In addition to the Geller's linelist, The Hirata–Horaguchi atomic spectral linelist [25] is used in an effort to try to identify new solar lines and to check their listed gf -values. Accurate databases of pure rotation and of vibration–rotation transitions are nowadays available for several molecular species as CO and its isotopic species, OH, and CN, but we had to create linelists for a few other species as yet unavailable (CH and NH) which were calculated either on the basis of accurate term values or on a set of spectroscopic constants adopting the most accurate transition probabilities then available. These databases enumerate a total of about 51 000 molecular lines which can also be used for the calculation of cool stellar spectra.

2.2.2. Synthetic solar spectra

Two synthetic spectra have been generated, one referenced to the disk center and the other referenced to a slant line-of-sight hitting the solar disk at 0.7 times the projected radius. The Holweger–Müller photospheric model [26] has been adopted in the calculations. A subset of the full astrophysical solar linelist (described below) has been used for these calculations, rejecting solar features with core absorption strengths below 0.01%. The condensed list still comprises about 33 230 molecular and atomic absorption lines between 700 and 5000 cm^{-1} . By combining this reduced astrophysical linelist with the synthetic spectra and the tables listing equivalent width, halfwidth and residual intensity of each line, a first guess of the empirical linelist can be constructed which tabulates line designation, wave number, line strength, half width and predicted parameters for center-to-limb variability for each line. The empirical model and the procedures applied to achieve further refinements of the empirical linelist are presented in Sections 3 and 4.

3. Setup of the empirical line-by-line model

The theory of line formation in the solar photosphere is beyond the scope of this article and is described elsewhere [27]. The details of physical mechanisms of line formation do not matter in the framework of an empirical model as developed here. However, an empirical model should take into account for the following physical characteristics:

- A solar absorption line is not expected to reach zero radiance in the infrared. The photospheric temperature minimum is about 4200 K, whereas the brightness temperature in the infrared continuum is about 5500 K,

depending on wave number. Therefore, a line becomes saturated when its fractional depth reaches the ratio of Planck radiances associated with these temperatures.

- Due to solar rotation, observed solar signatures have additional Doppler-broadening when the field of view covers a finite fraction of the solar disk.
- The relation between geometrical and optical depth along a chosen straight line that penetrates the photosphere depends on the inclination of the line with respect to the local perpendicular. Therefore, the continuum brightness temperature and especially the width and strength of spectral lines are expected to depend on the projected distance from solar disk center.
- A solar line does not emerge from a thin absorbing layer but is the sum of contributions over an interval of geometrical depth with considerable variation in pressure and temperature. Depending on transition probability and population of states, a variety of lineshapes can result. If thermal or turbulent broadening is dominating, the lineshape tends to be Gaussian, whereas damping processes add Lorentzian contributions to line wings falling off as $(\Delta\sigma)^{-2}$, in which $\Delta\sigma$ denotes the wave number difference from line center. The linear Stark broadening of hydrogen lines is a special case, since this process results in line wings falling off as $(\Delta\sigma)^{-5/2}$ [27, p. 219].

Important components of the model design are:

- parameterization of the shape of the lines,
- generation of the transmittance spectrum,
- accounting for the broadening due to solar rotation, and
- the extent of center-to-limb variation of lines and continuum brightness temperature.

The lineshapes of solar lines vary from near-Gaussian to Lorentzian up to cusp-shaped (sharper than a pure Lorentzian in the core). For ease of computation and to allow for the generation of cusp-shaped lines, an ad hoc parameterization of the shape $P_{A,b,w}(\Delta\sigma)$ according to Eq. (1) is used in preference to a Voigt profile. The distance from the line center measured in cm^{-1} is denoted by $\Delta\sigma$. The line is specified by three parameters: A gives the amplitude, $2b/\ln 2$ approximates the full-width at half-maximum, and w adjusts the shape from Gaussian ($w = 0$) via Lorentzian ($w = 1$) to a nearly cusp-shaped ($1 \leq w \leq 1.85$). Fig. 1 shows an array of curves generated with Eq. (1). Note that the half width of the profiles does not depend on w , but is constant to within 1% for any chosen value of the width parameter b . The numerical values in the equation are adjusted empirically to approximate the Lorentzian for $w = 1$ and to preserve constant half width for any

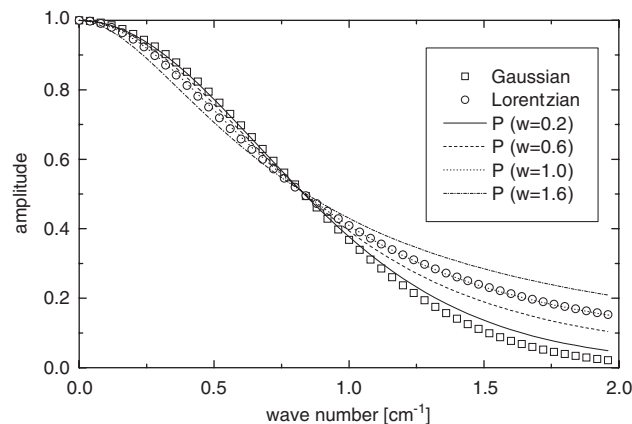


Fig. 1. Array of curves generated with Eq. (1) in comparison with Gaussian and Lorentzian curves. Full width at half-maximum of Gaussian and Lorentzian curves are $2\ln 2$. The choice $w = 0$ exactly reproduces the Gaussian and is therefore omitted. Values of w larger than 1 generate shapes which are narrower in the peak than a Lorentzian curve. We refer to these as ‘cusp-shaped’ curves.

choice of w

$$P_{A,b,w}(\Delta\sigma) = A \exp \left(- \frac{(\Delta\sigma)^2}{\sqrt{b^4 + w(-0.54b^4 + 0.33b^3|\Delta\sigma| + 0.12b^2(\Delta\sigma)^2 + 0.342b|\Delta\sigma|^3)}} \right). \quad (1)$$

The contributions to optical depth from all relevant lines $1, \dots, N$ are summed to yield the total optical depth τ at a given spectral position σ_0

$$\tau(\sigma_0) = \sum_{i=1}^N P_{A_i,b_i,w_i}(\sigma - \sigma_0). \quad (2)$$

The model transmittance $I(\sigma_0)$ is calculated via

$$I(\sigma_0) = I_\tau(\sigma_0) + [1 - I_r(\sigma_0)]e^{-\tau(\sigma_0)}, \quad (3)$$

defining a residual intensity $I_\tau(\sigma)$ as the ratio of two Planck curves $B(T)$

$$I_\tau(\sigma) = B(4000 \text{ K})/B(5140 \text{ K} + 0.28 \text{ K cm} \cdot \sigma). \quad (4)$$

This formulation takes into account that a maximum contrast cannot be exceeded. The introduction of such a kind of residual intensity was first proposed by Minnaert [28] in the treatment of solar absorption lines. The wave number-dependent brightness temperature in the denominator of Eq. (4) has been chosen to achieve good fit quality in the CO fundamental band covering $1600\text{--}2400 \text{ cm}^{-1}$ and to reproduce the levels of residual intensity found in the cores of the strongest solar lines in the 6000 cm^{-1} region.

Close inspection of the ground-based spectra recorded at Jungfraujoch indicates that the center-to-limb variation in the continuum brightness does not exceed a few per cent over the inner part of the solar disk. The center-to-limb variability found in strength and width of individual lines is moderate though detectable, so the model should allow for this possibility. Therefore, we assume that Eqs. (1)–(4) describe the calculation of the solar spectrum at any position of the projected disk, but allow for the line parameters A and b to vary as a function of projected disk radius ρ (0: center, 1: limb):

$$A(\rho) = A(0)(1 + V_A\rho^2), \quad (5)$$

$$b(\rho) = b(0)(1 + V_b\rho^2). \quad (6)$$

The empirical estimate of the center-to-limb variability for linestrength and line-width is contained in the parameters V_A and V_B , respectively. Finally, when expression (3) is evaluated at a certain position on the solar disk to match observations, the radial velocity between this volume element and the observer is to be taken into account. The Doppler shift modifies the spectral abscissa according to

$$\sigma_{\text{obs}} = \sigma_0(1 - v/c), \quad (7)$$

in which v and c denote the radial velocity and the speed of light, respectively. Algorithms to calculate the variable radial velocity between observer and center of the sun to the required accuracy are given in the astronomical literature [29]. In contrast, the treatment of Doppler contributions due to motions of the observed volume element with respect to solar center of inertia is not straightforward. Whereas the disk-projected Doppler pattern of a rigid rotating sphere (assuming the axis is oriented perpendicular to the line of sight) is a simple pattern of equidistant straight lines, the real situation is complicated by several factors: the solar equator is inclined with respect to the Earth orbit by about 8° , the solar rotation period increases towards the poles, and vertical as well as horizontal local motions are superimposed on the overall pattern [30]. However, as the broadening of the lines which results from the finite size of the field of view is smaller than the linewidth itself and the center-to-limb variation of the individual lines are moderate, the following simplified treatment is applied: to avoid a two-dimensional numerical integration, the field of view is divided into bands along the projected solar rotation axis. Eq. (3) is evaluated only once for each band and all contributions are summed applying weights proportional to each band length. To account for the center-to-limb variability of the lines, the spectrum is not calculated at the center of each band, but halfway towards the limit of the field of view.

This approach is equivalent to the rigid rotator assumption and approximates the integration of the spectrum along each band. A comparison with reference calculations performed by rigorous two-dimensional integration over surface elements of a non-rigid rotator demonstrates that the errors due to the simplified approach are below the typical error margins of the empirical model (see Section 5), so the additional computational effort is not justified. The line broadening contributions associated with local velocity dispersion in the solar atmosphere are consequently incorporated into the empirical linewidths and their center-to-limb variabilities. It should be noted that due to convective motions in the photosphere, the observed spectral positions of lines may be measurably shifted with respect to their nominal laboratory positions. In the case of CO, a shift between the cores of strong and weak lines of about 0.003 cm^{-1} is found [31]. Therefore, the line positions in an empirical linelist will differ slightly from the laboratory reference.

Finally, convective motions can introduce weak line asymmetries, so a possible extension of the empirical parameterization not included in this work might allow for asymmetric lineshapes. We note that significant progress has been made in the computation of lineshapes from first principles using modern radiative-hydrodynamical simulations of the solar photosphere [32]. However, especially in case of molecular lines, the calculation of linestrengths and lineshapes from first principles is still not fully achievable, since chemical reactions between different species impose tremendous complications [33].

4. Fit strategy

Given a suitable choice for the Minnaert offset (see Section 3), line parameters can be derived from the astrophysical linelist and the theoretical model spectra for the center and off-center positions on the solar disk (see Section 2.2). The resulting empirical linelist is then used to calculate an empirical spectrum.

For the comparison of an empirical spectrum with measured spectra, an interactive code which provides graphic output has been developed. The code generates plots which superimpose cleaned versions of the measured spectra in windows of adjustable size on the original measurement. The cleaned spectrum is generated by dividing each measurement by the empirical spectrum convolved with the applicable instrumental lineshape. Ideally, if the empirical model is perfect, then the cleaned spectra will have a flat smooth background and only the spectral features originating from the terrestrial atmosphere persist.

Before individual line parameters are changed ad hoc, it is preferable to exploit the knowledge associated with the astrophysical linelist. Therefore, in a first round of adjustment of the empirical line parameters, spectral bands originating from a common absorber are handled together and smooth functions of excitation energy of the lines and of spectral position are used to improve the empirical line parameters beyond the a priori estimate derived from the astrophysical model. The benefit of this approach is to project consistency to the empirical parameters as much as possible to lines of a certain species that are not easily accessible in the measured spectra. A practical illustration of this method is the fine tuning of the lineshape for solar CO lines in the fundamental band. The ground-based spectra offer the highest spectral resolution and therefore are used to determine the line width. However, due to interference with terrestrial absorbers not all CO lines are distinguishable in the measured spectra. Tuning only the accessible subset would lessen the consistency of the final set of empirical parameters, so instead all CO lines are uniformly adjusted to match the observations as close as possible. Common tuning of line parameters in this manner has been performed for bands of the prominent molecular absorbers OH, CO, NH, CH, and CN.

In a final step, individual line parameters are adjusted. The interactive code allows the selection of any line for manipulation of individual line parameters, the insertion of additional lines and the initiation of automatic iterative fits of all lines over specified spectral regions. In addition to measured and cleaned spectra, H₂O and CO₂ absorption spectra calculated for low pressure and $T = 300\text{ K}$ can be overlaid in the graphic display to readily identify those spectral positions where the ATMOS spectra show residual absorptions that are not of solar origin (see Section 2.1). Fig. 2 gives a sample of the graphical output of the computer program.

5. Results

The final spectrum contains 34 241 empirical lines between 700 and 5000 cm^{-1} . On the order of 1000 lines have been added to the astrophysical database and about 20 lines were removed as they seem to coincide with

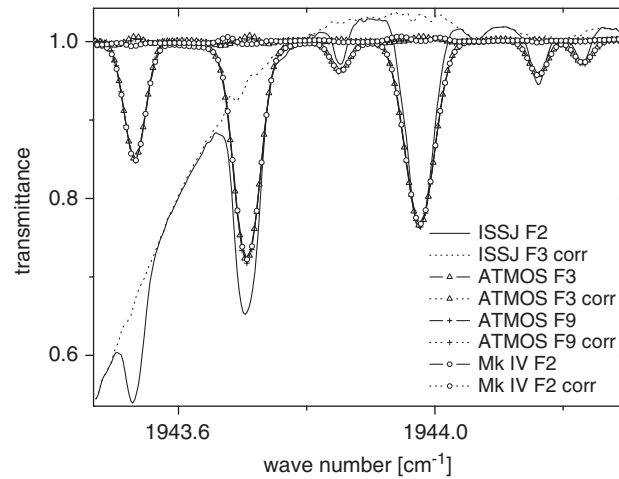


Fig. 2. Screen capture of interactive computer program for line manipulation. Several measurements before and after application of the empirical solar model are shown.

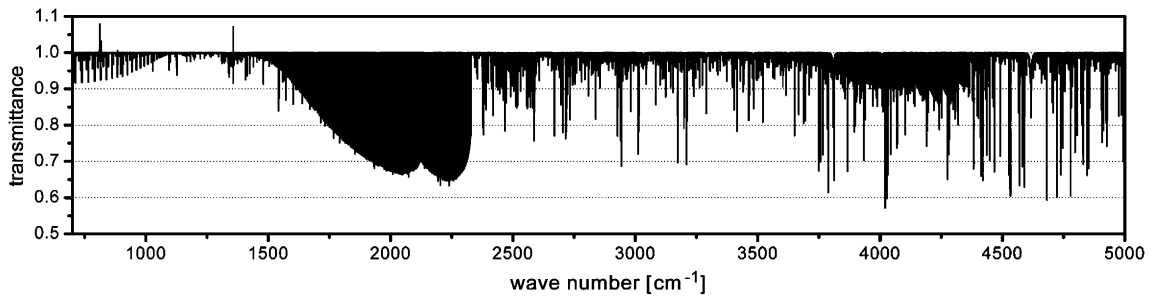


Fig. 3. The complete empirical solar spectrum, 700–5000 cm^{-1} (for solar disk center).

artifacts in the ATMOS spectra which were mistaken for solar lines. A small fraction of added empirical lines are not new lines of physical origin that are missing in the astrophysical database, but are merely introduced to improve the fit to the measured spectra in the case of strong lines with very complex shapes. The model decomposes such complex features into multiple line components (e.g. existence of an emission core or wide wings for H lines). Fig. 3 shows the resulting transmittance spectrum for the solar disk center over the complete spectral region covered by the model. The estimated accuracy of the empirical model achieved in the spectral transmission is in the order of 0.1% in the presence of isolated weak solar features, but worsens to 0.5% around strong lines and to 1% in blends of strong lines. The absolute accuracy of spectral positions for stronger unblended lines is of the order of a spectral scaling error of 2×10^{-6} , the consistency of relative positions within a spectral window of up to a few 10 cm^{-1} width is considerably better, a typical scatter in line positions of about 5×10^{-7} can be expected.

The linelist and the source code for the empirical solar model can be obtained from the first author. The model has been recently incorporated into the forward models of two spectral fitting codes, PROFFIT9 and SFIT2 [34], so these computer programs can be used to model solar absorption spectra including both terrestrial and solar features.

6. Verification

To demonstrate the performance of the empirical model, we use it to reproduce solar features in measurements which have not been used in the construction of the model. This is illustrated with spectra from three distinct measurement platforms: ground-based FTIR spectra recorded at Kiruna, Sweden [35], spectra of

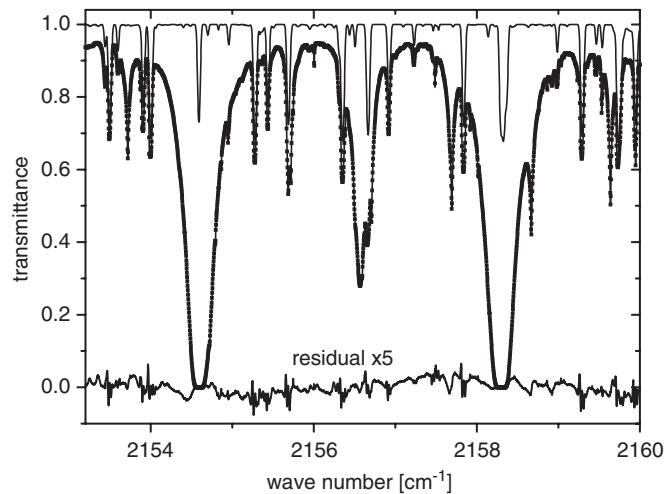


Fig. 4. Measured spectrum (dotted) and fit (line) including solar lines. The most prominent features are due to terrestrial CO. Many weaker lines are of solar origin. For identification the empirical solar spectrum is overlaid (top curve). The difference between measured and calculated spectrum is enlarged by a factor of 5 (bottom line). The measurement has been taken with the Bruker 120 HR FTIR located at IRF, Kiruna on March, 23, 2002.

the balloon-borne spectrometer operated by the University of Denver (DU) [8] and recent preliminary space-borne solar spectra from the ACE FTS [12]. Fig. 4 shows one out of four spectral windows used for the joint retrieval of terrestrial CO and OCS from ground-based spectra, selected from a standard solar measurement taken for NDSC purposes. The saturated lines are due to terrestrial CO, but most of the weaker lines are of solar origin. The residual shows evidence of lineshape mismatch around the solar features on the order of 0.5% rms error in transmission. This is due to residual discrepancies in linewidth between the measurement and the empirical model and also results from the slight asymmetry in the shape of the strongest solar lines that is well resolved in the high-resolution ground-based spectra. The wings of strong lines appear slightly steeper on the low wave number side.

During 1985–1995, the University of Denver (DU) balloon-borne FTIR system (based on a commercial Bomem spectrometer, model DA3.002) provided a unique set of solar absorption spectra. The spectra were recorded at 0.003 cm^{-1} resolution, from balloon altitudes of 35–38 km, at both high and low sun geometries. While the solar features at 0.003 cm^{-1} do not show significantly more details than the ATMOS 0.02 cm^{-1} resolution spectra, the study of the DU long path spectra continues to reveal previously unknown spectral features of stratospheric molecules. In most spectral regions of interest quantitative analysis of the spectral features requires accurate modelling of the solar background spectra. Portions of these spectra have been presented in the ongoing DU stratospheric atlas project [36], and in studies dedicated to various newly observed spectral features. Recent studies have focused on the $5\text{ }\mu\text{m}$ region, and led to significant revisions of the line parameters used for modelling the atmospheric spectrum in this region [37–39].

Fig. 5 displays the $2055.0\text{--}2057.5\text{ cm}^{-1}$ region from a scan recorded with a long path through the ozone layer, with simulations of the individual spectral components, using the latest HITRAN database [40]. Coverage of a wide region from a set of the flight scans in the $5\text{ }\mu\text{m}$ region is shown in the atlas [36], along with the molecular identification tables. Usually, 8–9 molecular species contribute significant line structure to the observed atmospheric spectra.

Fig. 6 displays a spectral fitting, using the SFIT2 code (v.391.2), in a sub-interval of Fig. 5 for $2055.4\text{--}2056.4\text{ cm}^{-1}$. The quality of the fitting varies across the range of Fig. 6, mostly due to the incomplete modeling of the ozone line parameters. The modeling of the solar component, in this spectrum and for spectra with smaller solar zenith angle, fits the observations well, significantly better than the ozone lines. In particular, the feature at 2056.2610 cm^{-1} , superimposed on the broader solar lines, is still unidentified, and listed with a question mark in the atlas tables. Further work on improvements of the ozone line parameters is in progress, as indicated in Refs. [39,40].

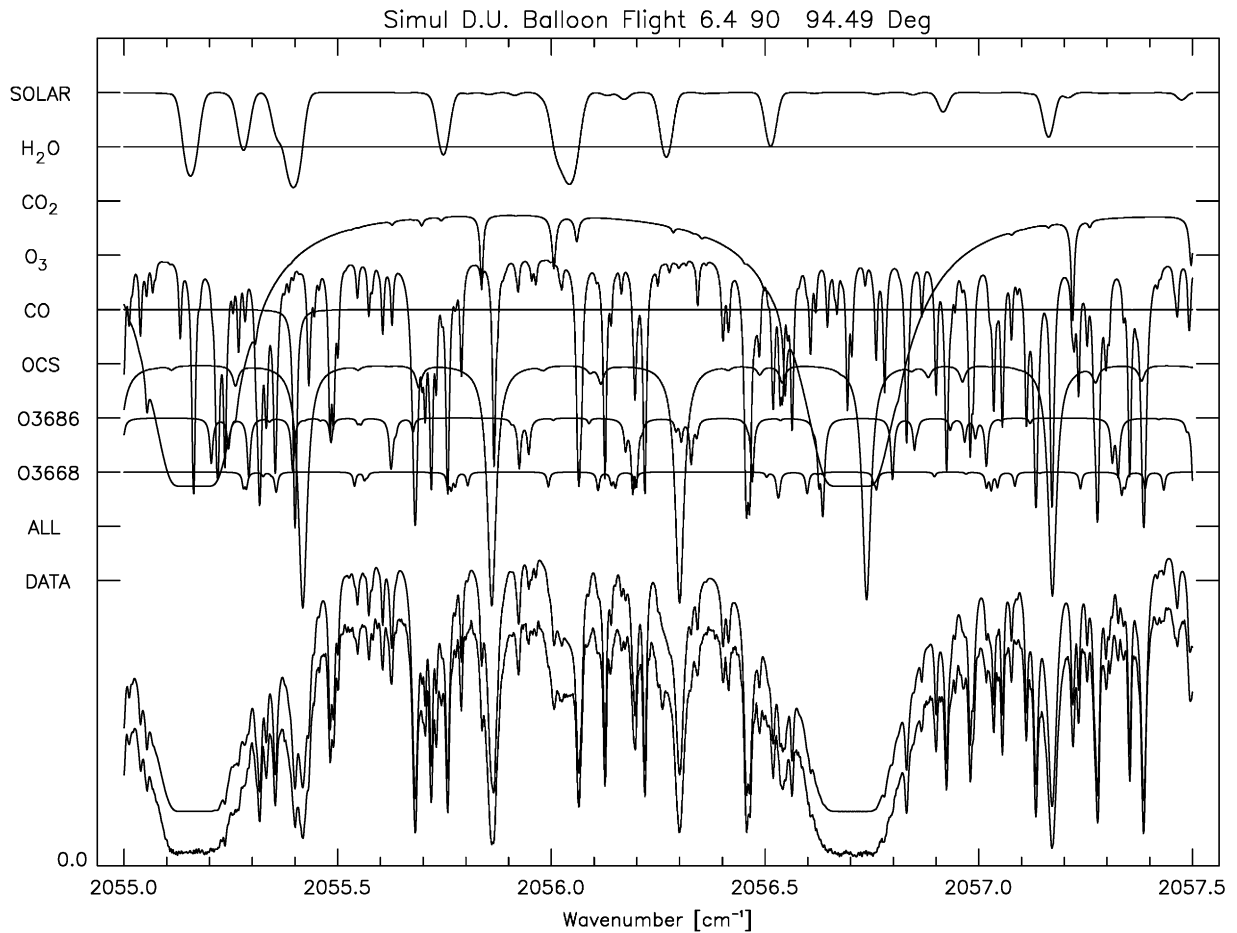


Fig. 5. Measured spectrum (bottom) and calculated spectrum (shifted upward). In the upper part of the figure the assignments of individual absorptions are given. Measurements were taken with the University of Denver balloon-borne FTIR system. For details see text.

The ACE FTIR [36] has the potential to greatly improve our knowledge of the infrared solar spectrum, especially with respect to very weak features which are not accessible at the SNR achieved in solar observations thus far. It should be noted that the preliminary spectra used here have been generated by co-adding only a small subset (three days of high sun spectra recorded in May 2004) of all available solar spectra and the baseline is not yet corrected for channelling which is present in the unratiod solar spectra. In addition, the individual solar spectra were not corrected for the change in the relative satellite–sun velocity, which introduced some additional line broadening through the Doppler effect. The maximum optical path difference for an ACE interferogram is limited to 25 cm (corresponding to a resolution of about 0.025 cm^{-1} for the full-width at half-maximum of the instrument lineshape function), therefore, the solar spectrum is not fully resolved. No numerical apodization has been applied in this intercomparison, and therefore narrow lines show some ringing. The model spectrum has been convolved with the nominal instrumental lineshape of ACE and the model spectral abscissa has been scaled by 1.0002778 to match the measured spectra in both the longwave HgCdTe as well as in the shortwave InSb regions. Fig. 7 covers a spectral window in the HgCdTe band of ACE, which contains weak solar features. The broader lines are atomic lines due to Mg I, the narrow lines are due to CO. Relative line positions, line widths and intensities are well captured by the model. Fig. 8 covers a region in the InSb band of ACE which is not accessible in ground-based spectra. All measured spectral features, mainly due to CO, are well reproduced in the empirical model. Fig. 9 gives an example in the shortwave region of the ACE InSb band. Most lines are due to CO, Mg I and Si I. Again, the agreement between measurement and empirical model is excellent.

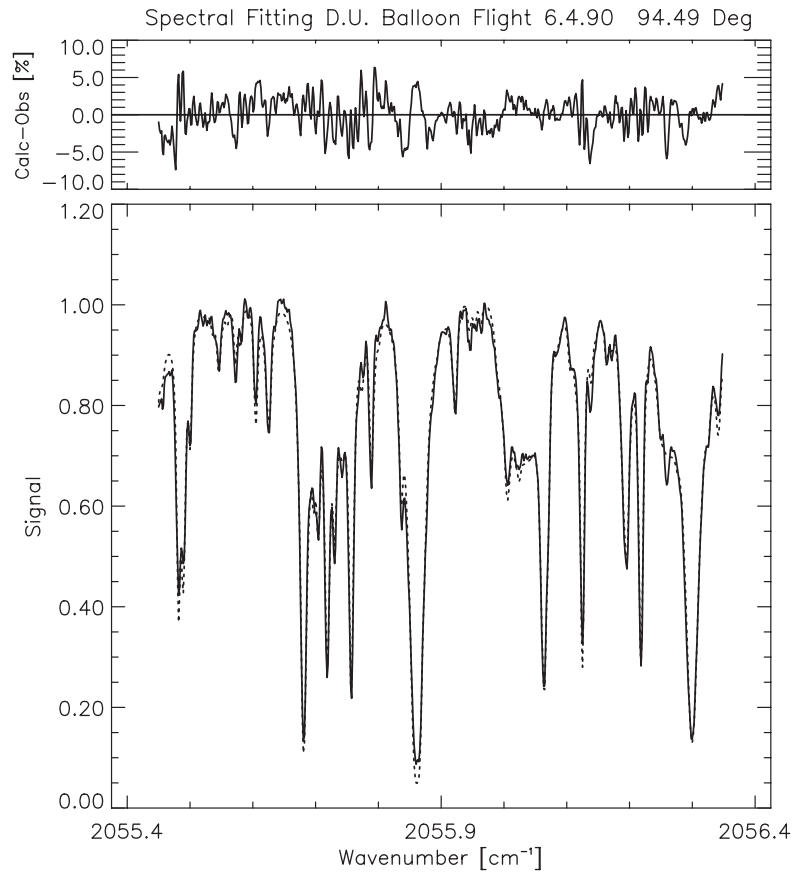


Fig. 6. Details of spectral window shown in Fig. 5. Measurements were taken with the University of Denver balloon-borne FTIR system. For details see text.

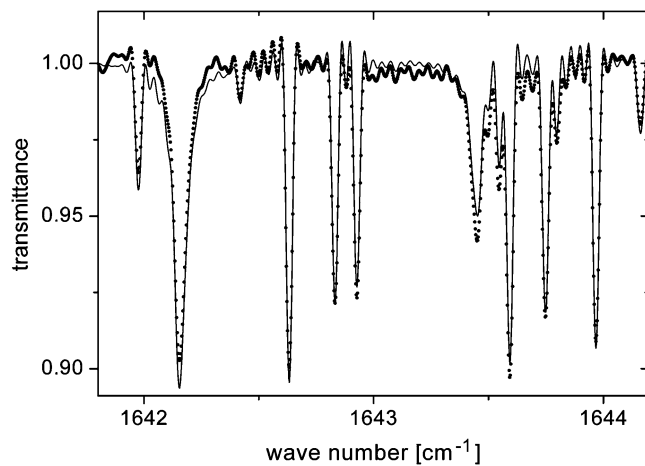


Fig. 7. Model intercomparison with ACE FTS measurements. Close up on MCT region. Smooth line: empirical model, dots: ACE.

7. Conclusion and outlook

The empirical line-by-line model presented here can be used to calculate the solar transmittance with high spectral resolution in the mid-infrared for remote sensing applications and investigations of radiative transfer

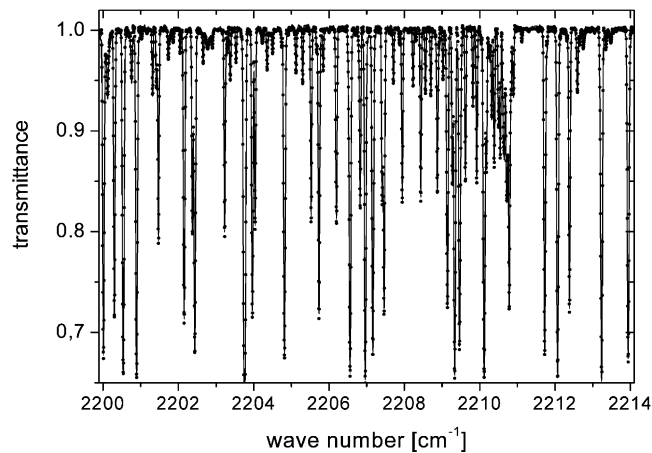


Fig. 8. Model intercomparison with ACE FTS measurements. Close up on InSb region inaccessible from ground. Smooth line: empirical model, dots: ACE.

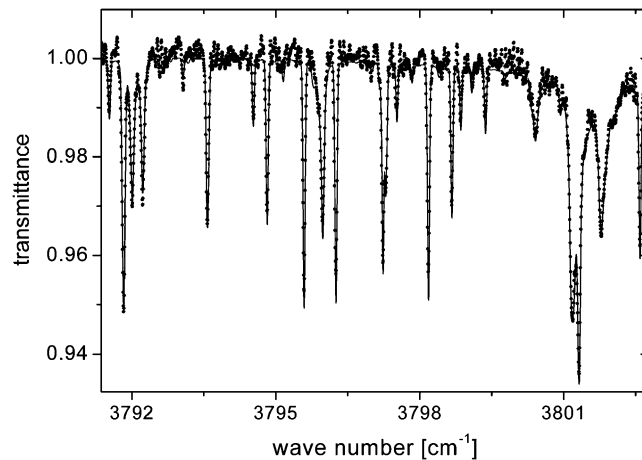


Fig. 9. Model intercomparison with ACE FTS measurements. Close up on InSb region. Smooth line: empirical model, dots: ACE.

in the terrestrial atmosphere. Preliminary extensions of the model towards the near infrared are already available, although the accuracy is expected to be worse in this spectral region due to a more limited observational database. By the use of the model within the NDSC FTIR community as well as by including new observational material of the solar spectrum, further improvements and extensions of the model are to be expected. Hopefully, solar absorption measurements from balloon-borne FTIR spectrometers calibrated to absolute radiances will be available in the near future. This will allow modelling the absolute solar radiance with high spectral resolution instead of the solar transmittance, which assumes spectral lines on a smooth continuum and does not cover variations of the continuum itself.

Acknowledgment

We wish to express our appreciation to the ATMOS Science Team and the Space Shuttle crews for the acquisition of high-quality exo-atmospheric spectra. We also thank the JPL Mk IV Interferometer Team, and the launch crews who contributed to the successful balloon flights. Part of this research was performed at the Jet Propulsion Laboratory under contract with NASA. The ACE mission is supported by the Canadian Space Agency and the Natural Sciences and Engineering Research Council of Canada. Data reduction for the preliminary ACE solar spectra were carried out by S. McLeod, R. Skelton and P. Sheridan. Work at the

University of Liège was primarily funded by the federal Office for Scientific, Technical and Cultural Affairs (OSTC) and by the European Commission-Directorate General (EC-DG), both in Brussels. Acknowledgements are further extended to the Jungfrauoch Stiftungsrat, for hosting the Liège laboratory. Work at the University of Denver was supported in part by NSF and NASA. At the National Center for Atmospheric Research (NCAR) we gratefully acknowledge the support of the National Science Foundation (NSF) and the National Aeronautics and Space Administration (NASA).

References

- [1] Fischer H, Hase F. Observations for chemistry (remote sensing) IR/FIR. In: Holton J, Pyle J, Curry J, editors. Encyclopedia of atmospheric sciences. Amsterdam: Elsevier; 2003. p. 1499–508.
- [2] Kurylo MJ. Network for the detection of stratospheric change (NDSC). In: Proceedings SPIE—the international society for optical engineering, vol. 1491; 1991. p. 168–74.
- [3] Kurylo MJ, Zander R. The NDSC—its status after 10 years of operation. Proceedings of the XIX quadrennial ozone symposium. Hokkaido University Sapporo, Japan, July 3–8, 2000. p. 167–8; Kurylo MJ. 10 years of the network for the detection of stratospheric change, NDSC symposium, September 24–27, 2001, Arcachon, France.
- [4] (<http://www.ndsc.ws/>).
- [5] Rinsland CP, Zander R, Demoulin P. Ground-based infrared measurements of HNO₃ total column abundances: long-term trend and variability. *J Geophys Res* 1991;96:9379–89.
- [6] Rinsland CP, Mahieu E, Zander R, Jones NB, Chipperfield MP, Goldman A, et al. Long-term trends of inorganic chlorine from ground-based infrared solar spectra: past increases and evidence for stabilization. *J Geophys Res* 2003;108(D8):4252 ACH10, doi:10.1029/2002JD003001.
- [7] Pougatchev NS, Jones NB, Connor BJ, Rinsland CP, Becker E, Coffey MT, et al. Ground-based infrared solar spectroscopic measurements of carbon monoxide during 1994 MAPS flights. *J Geophys Res* 1998;103:19317–25.
- [8] Murcray FJ, Kosters JJ, Blatherwick RD, Olson J, Murcray DG. High resolution solar spectrometer system for measuring atmospheric constituents. *Appl Opt* 1990;29:1520–5.
- [9] Toon GC, Blavier JF, Sen B, Margitan JJ, Webster CR, May RD, et al. Comparison of MkIV balloon and ER-2 aircraft measurements of atmospheric trace gases. *J Geophys Res* 1999;104:26779–90.
- [10] Camy-Peyret C, Jeseck P, Hawat T, Durry G, Payan S, Berub G, et al. The LPMA balloon-borne FTIR spectrometer for remote sensing of atmospheric constituents, vol. 370. European Space Agency Publication SP; 1995. p. 323–8.
- [11] Gunson MR, Abbas MM, Abrams MC, Allen M, Brown LR, Brown TL, et al. The atmospheric trace molecule spectroscopy (ATMOS) experiment: deployment on the ATLAS space shuttle missions. *Geophys Res Lett* 1996;23:2333–6.
- [12] Bernath PF, McElroy CT, Abrams MC, Boone CD, Butler M, Camy-Peyret C, et al. Atmospheric chemistry experiment (ACE): mission overview. *Geophys Res Lett* 2005;32:L15S01, doi:10.1029/2005GL022386.
- [13] Funke B, Martin-Torres FJ, Lopez-Puertas M, Höpfner M, Hase F, Lopez-Valverde M, et al. A generic non-LTE population model for MIPAS-ENVISAT data analysis, *Geophys. Res. Abstracts*, abstracts of the Contributions of the European Geophysical Society, Nice, France, 21–26 April 2002, CD-ROM, ISSN:1029-7006, 2002.
- [14] Höpfner M. Study on the impact of polar stratospheric clouds on high resolution mid-IR limb emission spectra. *JQSRT* 2004;83:93–107.
- [15] Abrams MC, Goldman A, Gunson MR, Rinsland CP, Zander R. Observation of the infrared solar spectrum from space by the ATMOS experiment. *Appl Opt* 1996;35:2747–51.
- [16] Farmer CB, Norton RH. A High-resolution Atlas of the infrared spectrum of the Sun and the Earth atmosphere from space. In: *The Sun*, vol. I. NASA Reference Publication 1224, 1989.
- [17] Abrams MC, Toon GC, Schindler RA. A practical example of the correction of Fourier transform spectra for detector nonlinearity. *Appl Opt* 1994;33:6307–14.
- [18] Toon GC. The JPL MkIV interferometer. *Opt Photonics News* 1991;2:19–21.
- [19] Demoulin P, Farmer CB, Rinsland CP, Zander R. Determination of absolute strengths of N₂ quadrupole lines from high resolution ground based IR solar observations. *J Geophys Res* 1991;96:13003–8.
- [20] Schneider M, Blumenstock T, Chipperfield M, Hase F, Kouker W, Reddmann T, et al. Subtropical trace gas profiles determined by ground-based FTIR spectroscopy at Izaña (28°N, 16°W): five year record, error analysis, and comparison with 3D-CTMs. *Atmos Chem Phys* 2005;5:153–67.
- [21] Sauval AJ. Atomic and molecular database of solar line parameters from 1 to 40 micron (250 to 10000 cm⁻¹): computer file [work in progress, September 2005]. E-mail contact: jacques.sauval@oma.be
- [22] Decin L. Synthetic spectra of cool stars observed with the ISO short-wavelength spectrometer: improving the models and the calibration of the instrument. PhD thesis, Katholieke Universiteit Leuven, May 2000.
- [23] Decin L, Waelkens C, Eriksson K, Gustafsson B, Plez B, Sauval AJ, et al. ISO-SWS calibration and the accurate modelling of cool-star atmospheres I. Method. *Astron Astrophys* 2000;364:137–56 II. General results, *Astron Astrophys* 2003;400:679–94. III. AO to G2 stars, *Astron Astrophys* 2003;400:695–707. IV. G9 to M2 stars, *Astron Astrophys* 2003;400:709–27.
- [24] Geller M. Key to identification of solar features from 650 to 4800 cm⁻¹. In: *A high resolution Atlas of the infrared spectrum of the Sun and the Earth atmosphere from space*, vol. III. NASA Reference Publication 1224, National Aeronautics and Space

- Administration, Washington DC, 1992; In: Sauval AJ, Blomme R, Grevesse N, editors. Laboratory and astronomical high resolution spectra. ASP conference series, vol. 81. 1995. p. 88–101 (2400 identified lines); unpublished results, 1998 (2700 identified lines).
- [25] Hirata R, Horaguchi T. Atomic spectral line list, 1995 (<http://vizier.u-strasbg.fr/cgi-bin/VizieR>, select “atomic data”, VI/69).
- [26] Holweger H, Müller E. The photospheric barium spectrum: solar abundance and collision broadening of Ba II lines by hydrogen. *Solar Phys* 1974;39:19–30.
- [27] Gray DF. The observation and analysis of stellar photospheres. Cambridge Astrophysics Series. Cambridge: Cambridge University Press; 1992.
- [28] Minnaert M. Die Profile der äusseren Teile der starken Fraunhoferschen Linien. *ZS F AP* 1935;10:40–51.
- [29] Meeus J. Astronomical algorithms. Richmond, Virginia: Willmann-Bell; 1991.
- [30] Stix M. The Sun, 2nd ed. Berlin, Heidelberg: Springer; 2002.
- [31] Farrenq R, Guelachvili G, Sauval AJ, Grevesse N, Farmer CB. Improved Dunham coefficients for CO from infrared solar lines of high rotational excitation. *J Mol Spectros* 1991;149:375–90.
- [32] Asplund M, Grevesse N, Sauval AJ, Allende Prieto C, Blomme R. Line formation in solar granulation VI. [CI], CI, CH and C₂ lines and the photospheric C abundance. *Astron Astrophys* 2005;431:693–705.
- [33] Wedemeyer-Böhm S, Kamp I, Bruls J, Freytag B. Carbon monoxide in the solar atmosphere: I numerical method and two-dimensional models. *Astron Astrophys* 2005;438:1043–57.
- [34] Hase F, Hannigan JW, Coffey MT, Goldman A, Höpfner M, Jones NB, et al. Intercomparison of retrieval codes used for the analysis of high-resolution ground-based FTIR measurements. *JQSRT* 2004;87:25–52.
- [35] Kopp G, Berg H, Blumenstock T, Fischer H, Hase F, Hochschild G, et al. Evolution of ozone and ozone related species over Kiruna during the THESEO 2000—SOLVE campaign retrieved from ground-based millimeter wave and infrared observations. *J Geophys Res* 2003;108(D5):8308–19.
- [36] Goldman A, Blatherwick RD, Kusters JJ, Murcray FJ, Murcray DG. Line positions and identifications. In: Atlas of very high resolution stratospheric IR absorption spectra, vol. I, The spectra, vol. II. Department of Physics, University of Denver, May 2005 edition. Also see (<http://www.du.edu/agoldman/atlas.html>).
- [37] Goldman A, Coffey MT, Stephen TM, Rinsland CP, Mankin WG, Hannigan JW. Isotopic OCS in the troposphere and lower stratosphere determined from high resolution infrared solar absorption spectra. *JQSRT* 2000;67:447–55.
- [38] Goldman A, Rinsland CP, Perrin A, Flaud J-M, Barbe A, Camy-Peyret C, et al. Weak ozone isotopic absorption in the 5 μm region from high resolution FTIR solar spectra. *JQSRT* 2002;74:133–8.
- [39] Goldman A, Barbe A, Tyuterev VIG, De Backer-Barilly M-R, Hannigan JW, Coffey MT, et al. Enhanced absorption lines of 16O₃ in the 5 μm region from high-resolution FTIR solar spectra. *JQSRT* 2005;96:241–50.
- [40] Rothman LS, Jacquemart D, Barbe A, Benner DC, Brown LR, Carleer MR, et al. The HITRAN 2004 molecular spectroscopic databases. *JQSRT* 2005;96:139–204.